Macromolecules

Article

Cite This: Macromolecules 2019, 52, 6792−6800

pubs.acs.org/Macromolecules

Effects of Side Chains on Polymer Knots

Liang Dai,[†] Beatrice W. Soh,[‡] and Patrick S. Doyle*[,‡]

[†]Department of Physics, City University of Hong Kong, 83 Tat Chee Avenue, Kowloon, Hong Kong, China

[‡]Department of Chemical Engineering, Massachusetts Institute of Technology, Cambridge, Massachusetts 02139, United States

Supporting Information

ABSTRACT: As an intriguing phenomenon, knotting in DNA, proteins, and other molecules has been extensively investigated in recent years, not only because of fundamental interest in knotting but also because of significant effects of knotting on mechanical, rheological, chemical, and biological properties. Some polymers contain side chains, and the effects of side chains on polymer knots are not clear. In this work, we investigate the effects of side chains on knots through Langevin dynamics simulations of knot diffusion along a stretched polymer with side chains. When the gap between side chains is larger than the knot size; each side chain acts as a barrier to slow down the knot diffusion. We find that how a knot crosses the barrier by a side chain resembles how a polymer translocates a pore. Inspired by the latter, we find a simple empirical expression for the free energy barrier caused by a side chain: $F_{barrier}/k_BT \approx 75R_g/L_{knot}$, where k_B is the Boltzmann constant, T is the temperature, R_g is the radius of gyration of a side chain, and L_{knot} is the contour length of the knot core. The equations and numerical results obtained in this work can guide the rational control of knot diffusivity along a polymer by side chains. In addition, our results provide insights into the understanding of knots in peptides and single-stranded DNA where side chains are common. Furthermore, this work makes a connection between two interesting phenomena for polymers—knotting and pore translocation.

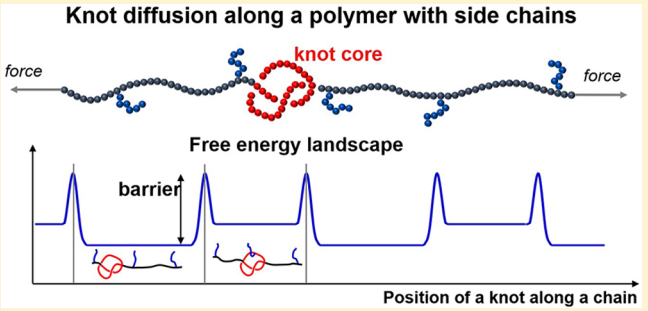

1. INTRODUCTION

Knotting is a common phenomenon that occurs in a wide range of linear objects, including headphone cords, DNA,[1,2] proteins,[3−7] and other molecules.[8,9] Recent studies have revealed that knotting can significantly affect polymer behavior, such as reducing mechanical strength of polymers,[10] slowing down polymer dynamics,[11,12] jamming nanopore translocation[13] and DNA ejection from virial capsids,[14−17] and facilitating catalysis of proteins.[5] To understand the general behavior of polymer knots, extensive simulation studies have been performed to investigate conformations and dynamics of knots using simple polymer models.[18,19] These simulation results have been used to explain experimental results, facilitate theoretical studies, and reveal novel phenomena of polymer knots. Monte Carlo simulations have been successfully applied to explain DNA knotting probability as a function of the salt concentration observed in experiments.[1,2] Monte Carlo simulations and Langevin dynamics simulations have revealed the nonmonotonic effects of spatial confinement on the knotting probability and knot sizes,[20−23] while relevant experiments have been carried out to measure the DNA knot behavior in nanofluidic channels.[24] The simulations of polymers in confinement have also been applied to explain DNA knotting probability in virial capsids.[14,25,26] Langevin dynamics simulations[27] have been used to study the diffusion of different knot types under various stretching forces in order to explain the experimental results[28] of knot diffusion on a stretched DNA. In recent years, our group has applied Brownian dynamics simulations[29−32] to understand the experimental results[11,12,33] of DNA knots under extensional flows. There are also many other simulation studies to understand knot behavior under other situations,[34−38] e.g., in the presence of crowding[39] and during nanopore translocation.[13,40,41] In addition to explaining experiments, simulations of polymer knots have facilitated the theoretical work on the mechanism of knot formation.[42,43] The metastable tight knots observed in simulations have confirmed the formation mechanism of tight knots in semiflexible[44] and flexible polymers[45] through the entropic effect.

In this work, we perform simulations to investigate the effects of side chains on polymer knots. The motivation of this work is multifold. First, side chains are common in polymers, such as single-stranded DNA and proteins, but side chains are usually ignored in previous simulations with simple polymer models. Understanding the effects of side chains on polymer knots should provide insights into the behavior of knotted proteins. Second, side chains can be used as a tool to effectively control polymer knots. In particular, the numerical results and empirical expressions obtained in this work can guide the rational control of knot diffusivity along a polymer with side chains. Third, as presented later, how a knot crosses the barrier caused by a side

Received: July 8, 2019
Revised: August 16, 2019
Published: August 29, 2019

DOI: 10.1021/acs.macromol.9b01425
Macromolecules 2019, 52, 6792−6800

chain resembles how a polymer translocates through a pore. The surprising similarity between knotted polymers with side chains and nanopore translocation of polymers makes a connection between two phenomena of polymers—knotting versus pore translocation.

2. SIMULATION METHOD AND THEORY

2.1. Simulation Method of Knot Diffusion along a Stretched Polymer with Side Chains. We use the LAMMPS program[46] to perform Langevin dynamics simulations of single knotted polymers. A polymer is modeled as a string of beads connected by springs. To generate initial conformations for simulations we add a tail (straight line) to each side of a tight knot core to build a long linear knotted chain with a length of L_{chain} and then add side chains that are perpendicular to the main chain (Figure 1a). The side chains with a length of L_{side} are

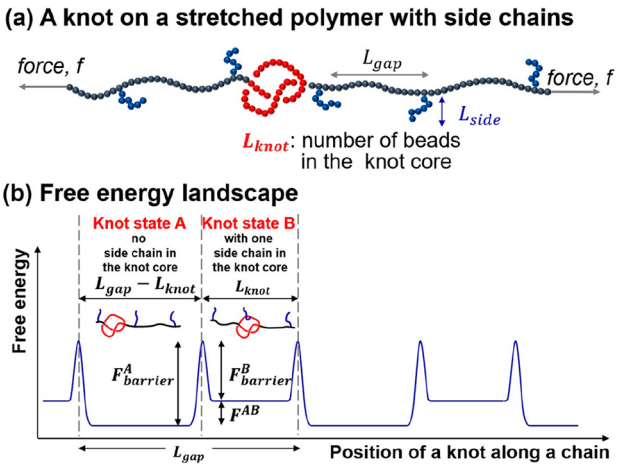

Figure 1. (a) Simulation setup. Knotted polymer is stretched by force, f. Side chains with the number of beads, L_{side}, are distributed evenly on the polymer backbone with a gap of L_{gap}. (b) Schematic illustration of the free energy landscape experienced by a knot during the diffusion along a polymer. There are two knot states. Knot state A is a knot with no side chain inside the knot core, while knot state B is a knot with one side chain inside the knot core. Transition between these two states requires the translocation of one side chain through the knot core and often requires overcoming a free energy barrier.

added uniformly on the main chain with a gap of L_{gap}. Stretching forces f are applied at both ends of the main chain. There are four parameters for each simulation: L_{chain}, L_{side}, L_{gap}, and f. We focus on knot diffusion along a long main chain far from the chain ends, and accordingly, the knot diffusion is independent of L_{chain}. As a result, there are only three parameters determining the knot diffusion: L_{side}, L_{gap}, and f.

The units of our simulations are as follows. We choose the style "unitless lj" in LAMMPS. In such style, we set the bead diameter a as the unit length, the bead mass m as unity, the Boltzmann energy k_BT as the unit energy, and the damping time α as unity. Here, k_B is the Boltzmann constant and T is the temperature. Then the diffusion coefficient of a single bead is $D_{bead} = 2k_BT\alpha/m = 2$ (in LAMMPS unit). The relaxation time of a single bead is $\tau_{bead} = a^2/D_{bead} = 0.5$ (in LAMMPS unit). As a result, τ_{bead} is one-half of the unit time in LAMMPS. We set the time step as $0.02\tau_{bead}$. In most simulations we run 10^{10} steps and save conformations every 10^5 steps for analysis. To visually inspect how a side chain enters and leaves a knot we save conformations every 10^3 steps ($20\tau_{bead}$) in certain simulations (e.g., Figure 5). For a given parameter set of (L_{chain}, L_{side}, L_{gap}, f), we usually use 10 random seeds to perform 10 independent simulations and calculate the average results of these simulations.

We usually set $L_{chain} = 1000a$, where a is the bead diameter treated as the unit length. We vary L_{side} from $6a$ to $36a$, L_{gap} from $50a$ to $150a$, and f from 0.5 to 1.5 k_BT/a, where k_B is the Boltzmann constant and T is the temperature. Because the computational cost is tremendous to explore the parameter space with varying L_{side}, L_{gap}, and f, we limit the current study to consider only the simplest knot type—the trefoil knot.

For a linear knotted polymer with two open ends, the knot can untie after diffusing to one end. Such untying process prevents us from observing knot dynamics over a long time in a simulation. To preserve the knotted state we perform additional simulations with a periodic boundary condition, which connects the two ends of a polymer at the boundary in the stretching direction. With this simulation setup, the polymer extension always equals the simulation box size in the stretching direction. As such, we do not need to impose the stretching force explicitly. The equivalent stretching force is the force that leads to the same polymer extension. The equivalent stretching force is adjusted by tuning the polymer extension, i.e., the simulation box size in the stretching direction. We find that the simulations in free space and simulations with a periodic boundary condition yield the same results of knot dynamics after mapping the stretching force to the polymer extension (simulation box size).

The pairwise interactions between beads are described by a purely repulsive Lennard−Jones potential

$$E_{LJ} = 4\epsilon_{LJ}\left[\left(\frac{\sigma}{r}\right)^{12} - \left(\frac{\sigma}{r}\right)^{6}\right] \quad (1)$$

with $\epsilon_{LJ} = 10\ k_BT$. We treat σ as the bead diameter, i.e., $a \equiv \sigma$. The cutoff of Lennard−Jones potential is set as $r_c = 2^{1/6}a \approx 1.1224a$ to produce a purely repulsive potential. For $r > r_c$, the pair interaction potential is zero. The bond interaction between adjacent beads is described by the FENE potential

$$E = -0.5KR_0^2 \ln\left[1 - \left(\frac{r}{R_0}\right)^2\right] + 4\epsilon_{bond}\left[\left(\frac{\sigma}{r}\right)^{12} - \left(\frac{\sigma}{r}\right)^{6}\right] + \epsilon_{bond} \quad (2)$$

where the maximum stretching distance R_0 is set as $1.5a$ and the stiffness of the bond is set by $K = 30\ k_BT$. We set $\epsilon_{bond} = 1\ k_BT$. These parameters are typical in the bead−spring model of polymers.

The knot type of the main chain is identified by calculation of the Alexander polynomial. Before calculation of the Alexander polynomial, all beads in the side chains are removed and only beads in the main chains are considered. In principle, calculation of the Alexander polynomial is strictly defined only for a circular chain. For an open linear chain, both ends usually need to be connected by a loop before calculation of the Alexander polynomial. However, for a substantially stretched chain in the current study, both ends are far away from the knot core and a connecting loop can be easily found without producing any additional crossing. To determine the boundary of the knot core, we cut beads one by one from each end of the chain until the topology changes. Then we determine the knot size L_{knot} as the number of beads within the knot core.

DOI: 10.1021/acs.macromol.9b01425
Macromolecules 2019, 52, 6792−6800

To calculate the knot diffusion coefficient we first determine the two boundaries of the knot core, denoted as p_{start} and p_{end}, which are the indices of the boundary beads on the main chain. The position of the knot on the main chain is defined as $p_{knot} = (p_{start} + p_{end})/2$. Note that we do not use the knot position in real space. Instead, we use the knot position on the main chain. Then the diffusion coefficient is calculated as $D_{knot} \equiv \langle p_{knot}(t + \Delta t) - p_{knot}(t)\rangle_T^2/\Delta t$.

2.2. Theory for the Effects of Side Chains on a Knot. Each side chain imposes a barrier for the knot diffusing along the main chain. As a result, a knot diffuses in a stepwise manner, which has been observed in our simulations. As shown in Figure 1b, a knot hops between states A and B, corresponding to polymer conformation without and with a side chain in the knot core. Supposing that the average lifetimes of a knot in the states A and B are τ_A and τ_B, respectively, we can derive the diffusion coefficient as

$$D = (L_{gap}/2)^2/[(\tau_A + \tau_B)/2] = L_{gap}^2/[2(\tau_A + \tau_B)] \quad (3)$$

because each hopping between the two states leads to a diffusion distance of $L_{gap}/2$ within an average time period of $(\tau_A + \tau_B)/2$. Now we proceed to the derivation of τ_A and τ_B. We focus on the regime where the free energy barrier caused by a side chain is substantially larger than the thermal energy k_BT. Accordingly, we can express τ_A and τ_B as

$$\tau_A = T_A \exp(F_{barrier}^A/k_BT) \quad (4)$$

$$\tau_B = T_B \exp(F_{barrier}^B/k_BT) \quad (5)$$

where T_A and T_B are the characteristic times of the knot staying in the two states in the absence of the free energy barrier (side chain). As shown in Figure 1b, in state B a knot diffuses over a distance of L_{knot}, and hence, we approximate T_B as

$$T_B \approx \langle L_{knot}\rangle^2/D_0 \quad (6)$$

where $\langle L_{knot}\rangle$ is the mean knot size and D_0 is the diffusion coefficient in the absence of side chains and solely depends on the stretching force. The characteristic time T_A is relatively more complicated. Our simulation results show that it is improper to approximate $T_A \approx (L_{gap} - L_{knot})^2/D_0$. Instead, our simulation results observe a linear relationship between τ_A and L_{gap} and suggest the expression

$$T_A \approx \langle L_{knot}\rangle(L_{gap} - \langle L_{knot}\rangle)/D_0 \quad (7)$$

The reason for the above expression is as follows. In state A with a large gap L_{gap}, the knot has an equal probability to be located anywhere within the gap except at the vicinity of side chains, which has been proven by our simulation results. Only when the position of the knot center is close to a side chain within a distance less than $\langle L_{knot}\rangle/2$, the knot has a chance to hop to state B. The relative probability of a knot with a distance less than $\langle L_{knot}\rangle/2$ from a side chain is $p_{vicinity} = \langle L_{knot}\rangle/(L_{gap} - \langle L_{knot}\rangle)$. When a knot in state A is close to a side chain, the characteristic time of hopping ignoring the free energy barrier is $T_{hop} = \langle L_{knot}\rangle^2/D_0$. Dividing this characteristic time by the probability of a knot being in the vicinity of a side chain, i.e., $T_A = T_{hop}/p_{vicinity}$, we arrive at eq 7.

Substituting eqs 4−7 into eq 3 and making an approximation that $F_{barrier}^A \approx F_{barrier}^B$ we obtain

$$D \approx D_0 \exp(-F_{barrier}^B)L_{gap}/(2\langle L_{knot}\rangle) \quad (8)$$

2.3. Simulation of the Pore Translocation of a Tethered Polymer. The diffusion coefficient of a knot on a polymer with side chains depends on the free energy barrier caused by a side chain. Such barriers are related to the translocation of a side chain through a hole within a knot. To obtain a better understanding of the barrier, we perform simple simulations for the translocation of a polymer through a pore (Figure 2). In the pore simulations we tether one end of a polymer inside a pore, which is different from typical simulations of pore translocation of a polymer.[47] The tethered end of the polymer is free to move within the pore, so that the situation is similar to the hopping between knot states A and B. The pore is built by fixed beads. We place the centers of N_{bead} touching beads along the perimeter of a circular pore with a diameter of $1/\sin(\pi/N_{bead})$. After excluding the space occupied by these beads themselves, the diameter of the pore is

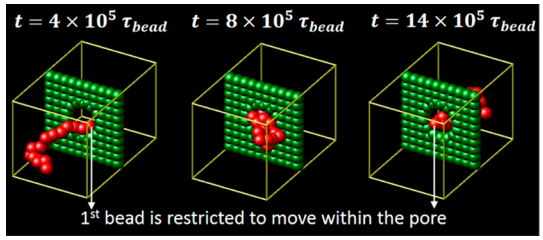

Figure 2. Simulation of the translocation of a tethered polymer through a pore. Green beads are fixed to build a pore during the simulation. Red beads correspond to a polymer. Three images are snapshots of conformations in the simulation with $D_{pore} = 3.49a$ and $L_{polymer} = 18a$.

$$D_{pore} = 1/\sin(\pi/N_{bead}) - 1 \quad (9)$$

We set N_{bead} as 13, 14, 15, 16, 18, 20, 22, 24, 26, 30, and 34 beads, corresponding to the pore diameter, D_{pore}, of 3.81a, 4.13a, 4.76a, 5.39a, 6.03a, 6.66a, 7.30a, 8.57a, and 9.84a, respectively.

3. RESULTS AND DISCUSSION

3.1. Simulation Results for a Knotted Polymer without Side Chains. We first present the simulation results for a chain without side chains in Figure 3. As the stretching force f increases, a knot becomes smaller and diffuses slower. We find that for $0.4\ k_BT/a < f < 10\ k_BT/a$ the dependence of $\langle L_{knot}\rangle$ on f can be approximated as

$$\langle L_{knot}\rangle/a \approx 28.8/f + 10.6 \quad (10)$$

We also find that for $0.4\ k_BT/a < f < 3\ k_BT/a$ the dependence of the diffusion coefficient of a trefoil knot, D_0, on f can be approximated as

$$D_0/(a^2/\tau_{bead}) \approx 1/(2.83f + 8.1) \quad (11)$$

In eqs 10 and 11, the force f is in units of k_BT/a. These empirical expressions provide convenience in the numerical calculation of knot sizes and the knot diffusivity in the absence of side chains, which are needed in the comparison between simulation results and theoretical predictions presented later. Our results quantitatively agree with the previous study[27] by Huang and Makarov. Here, we explore stretching forces as low as $f = 0.4\ k_BT/a$, while the previous study by Huang and Makarov used stretching forces $f \geq 2\ k_BT/a$.

3.2. Stepwise Diffusion of a Knot in Simulations. Now we proceed to the simulation results in the presence of side chains. Recall that we focus on a large-gap regime such that L_{gap}

DOI: 10.1021/acs.macromol.9b01425
Macromolecules 2019, 52, 6792−6800

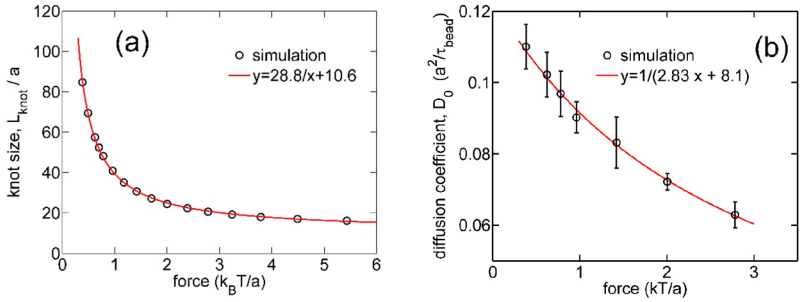

Figure 3. Mean knot size $\langle L_{knot} \rangle$ (a) and diffusion coefficient, D_0, of a knot (b) as a function of stretching force in the absence of side chains.

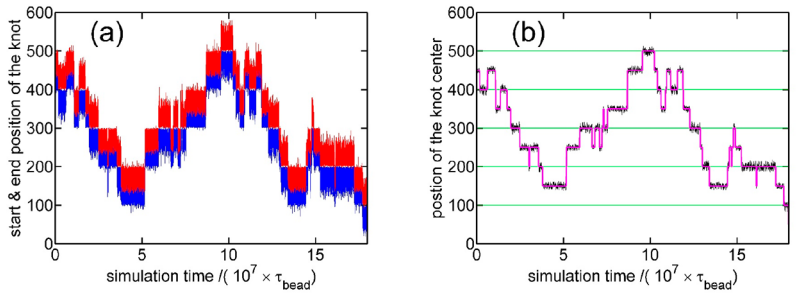

Figure 4. Stepwise diffusion of a knot in the simulation with $L_{side} = 25a$, $L_{gap} = 100a$, and $f = 0.7\ k_BT/a$. (a) Red and blue lines are the start and end positions of the knot core along the main chain, respectively. Each line consists of 90 000 data points saved with a time interval of $2000\tau_{bead}$ during a simulation. (b) Black line is the position of the knot center, which is the middle point of the start and end points and obtained by smoothing the data in a with a sliding window. Green lines are the locations of grafting sites on the main chain. Pink line is the stepwise position of the knot, which is either at the grafting sites or at the middle of two grafting sites.

> $\langle L_{knot} \rangle$. As a result, there is at most one side chain in the knot core. Figure 4a shows a typical stepwise diffusion of a knot. In this example, the stretching force is $f = 0.7k_BT/a$, corresponding to $\langle L_{knot} \rangle \approx 51.7a$. The gap is $L_{gap} = 100a$, which is roughly double of the equilibrium knot size $\langle L_{knot} \rangle$. The side chain length is $25a$. Due to barriers caused by the side chains, a knot is typically reflected many times by side chains before crossing the barrier and hopping from knot state A to B or vice versa (see Figure 1). For the convenience of identifying whether a knot is in state A and B, we smooth the trajectory of the knot diffusion using a sliding window with a size of $2000\tau_{bead}$ (50 data points). After smoothing, the knot center is usually located on the grafting sites of side chains or in the middle of two grafting sites with small fluctuations (Figure 4b). Such clear stepwise trajectory allows us to simply determine the state of a knot.

Figure 5 shows a series of polymer conformations during a hopping event. The hopping is realized by the translocation of a side chain through a pore (an open area) inside the knot. Prior to translocation the knot diffuses to the vicinity of the side chain. The translocation event occurs through the random motion of beads in side chains and knot cores. Note that we focus on the regime in which the free energy barrier is substantially larger than the thermal energy k_BT, and thus, the knot usually diffuses forth and back many times between two side chains before crossing a side chain. Accordingly, it is random which one of the two side chains is crossed by the knot.

Figure 6 shows the distributions of the knot positions in two states. In state A (no side chain in the knot core), the knot position distributes uniformly within the gap with a width of $L_{gap} - \langle L_{knot} \rangle$ between two side chains except at the vicinity of the side chains. Such uniform distribution results from the fact that the free energy of the knot is the same at every location, and the knot diffuses forth and back many times between the two side

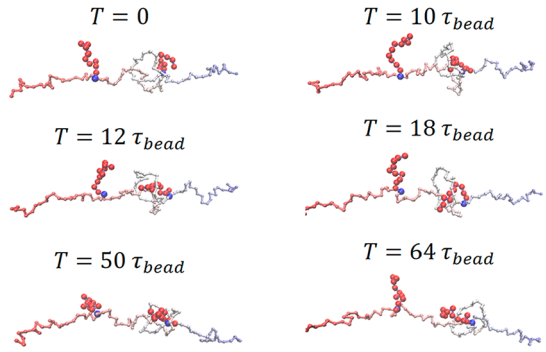

Figure 5. Translocation of a side chain that drives the knot from state A to B. Simulation parameters are $f = 1\ k_BT$, $L_{gap} = 50a$, and $L_{side} = 10a$. Backbone of the polymer is represented by beads and rods with gradually changing color. Side chains are represented by red beads. Grafting sites of side chains are represented by blue beads.

chains before crossing a side chain. In state B (one side chain in the knot core), the knot position distributes in a region with a width of $\langle L_{knot} \rangle$. It is worth pointing out that there are some overlap regions both knot states can reach, because a knot can push a side chain away but does not cross the side chain. The distribution of the knot position in Figure 6 agrees with the illustration in Figure 1b.

3.3. Lifetimes of Two Knot States. After determining the knot state during diffusion, we can identify hopping events and then calculate the dwelling time between two hopping events. Our analysis shows that the distribution of the dwelling times appears to follow an exponential decay (see the Supporting Information). A similar exponential decay was also observed in the previous study of knot translocation in a highly stretched

DOI: 10.1021/acs.macromol.9b01425
Macromolecules 2019, 52, 6792−6800

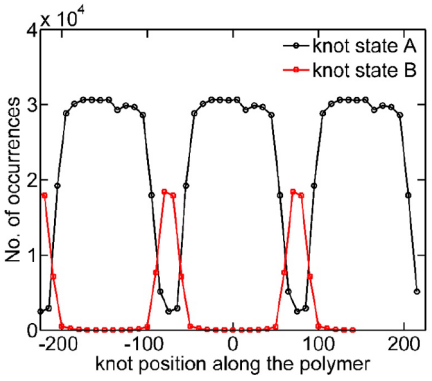

Figure 6. Distributions of knot position along the polymer in the simulation with $f = 1.5\ k_BT/a$, $L_{gap} = 150a$, and $L_{side} = 6a$.

chain.[48] We consider the average dwelling time as the lifetime of a knot state.

Figure 7 shows the dependence of the lifetimes of two knot states as a function of L_{gap}. The lifetime of state B is insensitive to L_{gap}, which is reasonable considering that knot state B (one side chain in the knot core) cannot feel the existence of other side chains as long as L_{gap} is sufficiently large. The lifetime of knot state A appears to have a linear relationship with L_{gap}, because a larger L_{gap} corresponds to a smaller probability of the knot staying in the vicinity of a side chain and only the knot in the vicinity of a side chain has a chance to hop. Such results support the approximation in eq 7. The linear relationships between τ_A and L_{gap} in Figure 7 are also consistent with the uniform distribution of knot position in Figure 6.

3.4. Free Energy Barrier Caused by a Side Chain. We estimate the free energy barrier caused by a side chain based on the lifetimes of two knot states using eqs 4 and 5 and the inputs of τ_A, τ_B, T_A, and T_B. We extract the lifetimes τ_A and τ_B from simulations and calculate the characteristic times T_A and T_B using eqs 6 and 7. The values of $\langle L_{knot}\rangle$ and D_0 can be estimated based on the empirical expression in eqs 10 and 11. Note that the presence of one side chain in a knot core makes the knot slightly larger than in the case of no side chains. We ignore the increase of knot size caused by the side chain because such an increase is quite small.

Figure 8 shows the free energy barriers as a function of side chain length. The free energy barriers typically range from 2 to 5 k_BT. For $F_{barrier} \gg 5\ k_BT$, the transition between the two knot states never occurs or occurs too few times in simulations such that we are unable to determine τ_A and τ_B precisely. For $F_{barrier} \ll 2\ k_BT$, the knot diffusion is no longer step-like but rather continuous. In this case, it is difficult to distinguish whether the knot is in state A or B and then difficult to calculate lifetimes and free energy barriers.

There are notable differences between $F^A_{barrier}$ and $F^B_{barrier}$, which are typically fractions of k_BT. The reason behind this difference is illustrated in Figure 1. In knot state B (one side chain in the knot core) there are excluded volume interactions (repulsions) between the side chain and the knot core, while in knot state A there are no such excluded volume interactions. As a result, knot state B has a higher free energy than knot state A and it is relatively easier to cross the barrier.

3.5. Diffusion Coefficient of a Knot. The presence of side chains slows down the long-time diffusion of a knot along a polymer. Figures 9a and 9b show the diffusion coefficient as a function of L_{gap} and L_{side}, respectively. We compare the simulation results to theoretical predictions by eq 8. Applying eq 8 requires the values of $\langle L_{knot}\rangle$, D_0, and $F^B_{barrier}$. The values $\langle L_{knot}\rangle$ and D_0 are given by the empirical expressions in eqs 10 and 11, respectively. The value of $F^B_{barrier}$ depends on f and L_{side}. We use another empirical expression in eq 17 to calculate $F^B_{barrier}$, which will be discussed later. Equation 8 predicts a linear relationship between D and L_{gap}, which agrees with the simulation results in Figure 9a. Equation 8 suggests that the dependence of D on L_{side} is through an exponential dependence on the free energy barrier $F^B_{barrier}$. Therefore, increasing L_{side} dramatically slows down the knot diffusion. Note that the derivation of eq 8 is based on an approximation that $F^A_{barrier} \approx F^B_{barrier}$.

3.6. Pore Translocation of a Tethered Polymer. We note that how a side chain translocates through a knot core resembles how a polymer translocates a pore. Because the latter case is relatively simpler, we perform simulations of pore translocation of a tethered polymer in order to obtain a simplified view of how a side chain translocates through a knot core. Note that in our simulations the first bead of the polymer is restricted to move within the pore, which is different from typical simulations of polymer translocation.[47] We focus on the hopping of the polymer between the two sides of the pore (see Figure 2 and the Supporting Information).

Because the pore is fixed, we can easily calculate the number of beads on each side (left or right side) of the pore at each time step. Figure 10a shows the histogram of the number of beads on the left side of the pore. Note that the first bead is restricted to move within the pore and is not considered to be on either the left or the right side of the pore. On the basis of the histogram we can calculate the polymer free energy using

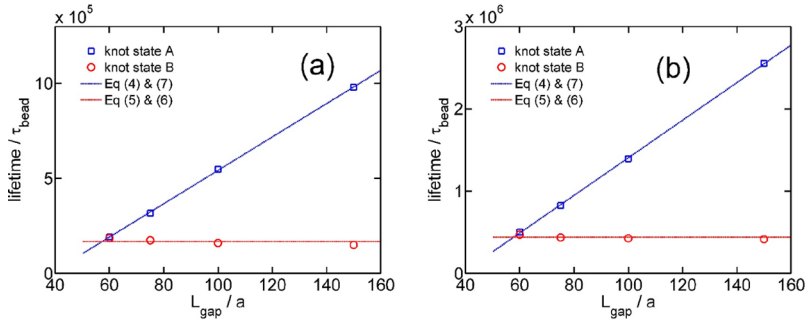

Figure 7. Lifetimes of two knot states as a function of L_{gap}. Simulation parameters are $f = 1.5\ k_BT/a$ and $L_{side} = 6a$ (a) and $f = 1.5\ k_BT/a$ and $L_{side} = 8a$ (b). Blue lines are based on the linear relationship between τ_A and L_{gap} in eq 7. Red lines are based on eq 6, where τ_B is independent of L_{gap}.

DOI: 10.1021/acs.macromol.9b01425
Macromolecules 2019, 52, 6792−6800

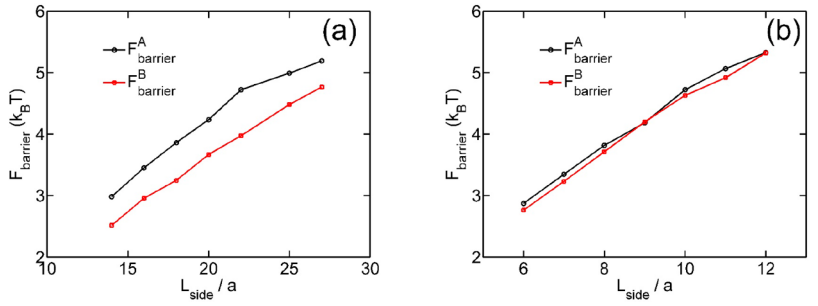

Figure 8. Free energy barriers for state A and B as a function side chain length. (a) Stretching force is $f = 0.7\ k_BT/a$. (b) Stretching force is $f = 1.5\ k_BT/a$.

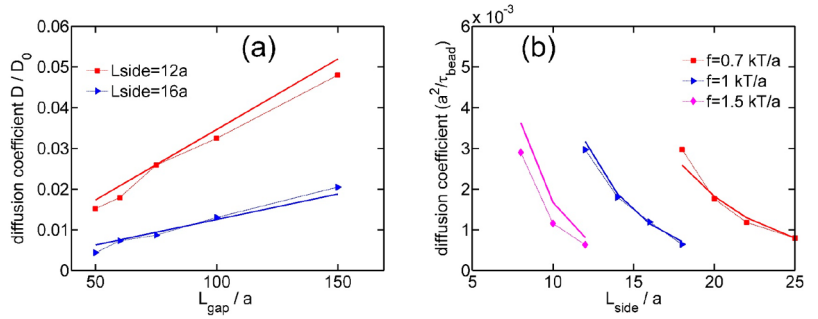

Figure 9. (a) Normalized diffusion coefficient of the knot as a function of L_{gap} for $f = 1\ k_BT/a$. Here, D_0 is the diffusion coefficient in the absence of side chains under the force $f = 1\ k_BT/a$. (b) Knot diffusion coefficient as a function of L_{side} when we fix $L_{gap} = 100a$. Thick solid lines in (a) and (b) are calculated from eq 8.

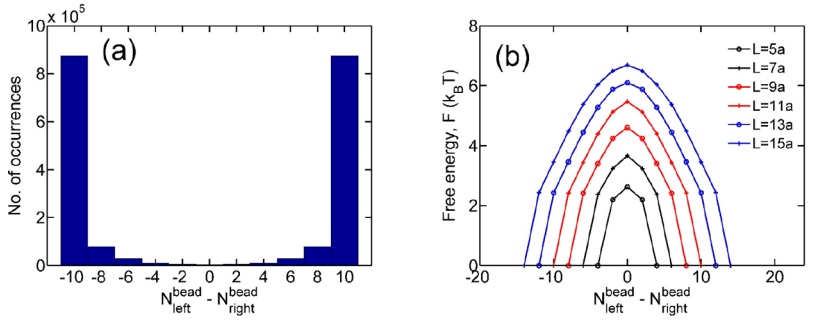

Figure 10. (a) Histogram of $N^{left}_{bead} - N^{right}_{bead}$ in the simulation with $L_{polymer} = 11a$ and $D_{pore} = 3.5a$. Here, $N^{left}_{bead} - N^{right}_{bead}$ is the difference in the number of beads located on the left and right sides of the pore. (b) Free energy as a function of $N^{left}_{bead} - N^{right}_{bead}$ for different polymer lengths.

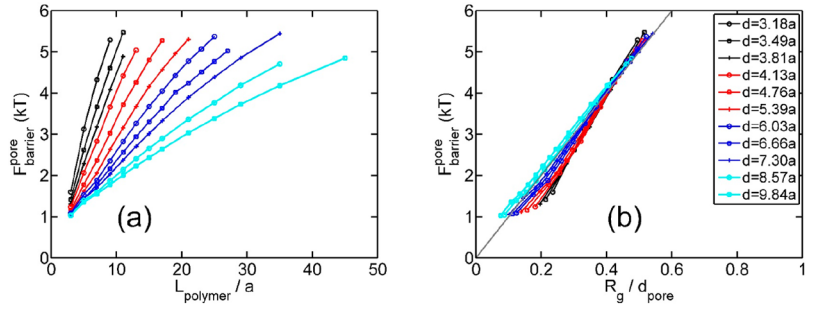

Figure 11. (a) Free energy barrier experienced by a polymer during pore translocation as a function of the polymer length. (b) Same data as (a) but replacing the chain length $L_{polymer}/a$ by the radius of gyration of the chain R_g/d_{pore}. Different colors and symbols represent different pore diameters. Perimeters of these circular pores are built by 13, 14, 15, 16, 18, 20, 22, 24, 26, 30, and 34 beads.

$$F_{polymer}/k_BT = -\ln(P(N^{left}_{bead})) \tag{12}$$

Figure 10b shows the free energy as a function of N^{left}_{bead}. The peak is located at $N_{left} = (L_{polymer} - 1)/2$. Then we define the free energy barrier as

$$F^{pore}_{barrier} = F_{polymer|N_{left}=(L_{polymer}-1)/2} - F_{polymer|N_{left}=0} \tag{13}$$

We calculate the free energy barrier for various pore diameters and polymer lengths (Figure 11). We find that the curves for different pore diameters substantially collapse when we replace

DOI: 10.1021/acs.macromol.9b01425
Macromolecules 2019, 52, 6792−6800

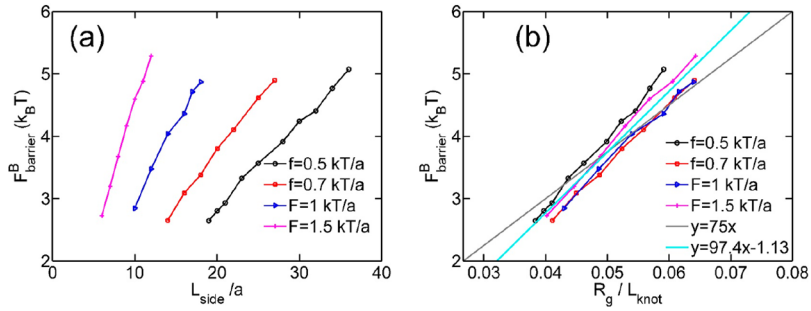

Figure 12. (a) Free energy barrier $F^B_{barrier}$ as a function of L_{side} for four stretching forces. (b) Free energy barrier $F^B_{barrier}$ as a function of R_g/L_{knot} for four stretching forces.

$L_{polymer}$ by R_g/D_{pore}, where R_g is the average radius of gyration of the polymer. For the convenience of the numerical calculation we find an empirical expression to calculate the radius of gyration of a polymer with a length between $2a$ and $50a$ based on our simulations

$$R_g \approx 0.355 \times L^{0.678} \tag{14}$$

Note that due to the wall around the pore, the tethered polymer has a radius of gyration slightly larger than that of the polymer with the same length in free space (see the Supporting Information). The collapsed curves appear to roughly follow the linear relationship

$$F^{pore}_{barrier} \approx 10R_g/d_{pore} \tag{15}$$

3.7. Comparison of Free Energy Barriers in Knot Diffusion and Pore Translocation. The master curve in Figure 11b inspires us to analyze the free energy barrier caused by the side chain in a knotted polymer. Now we replace the pore diameter by the knot size. Figure 12 shows the four curves for different stretching forces indeed substantially collapse when we plot $F^B_{barrier}$ as a function of R_g/L_{knot}. The best fit to the simulation data points yields the following two equations using one or two fitting parameters

$$F^B_{barrier}/k_BT \approx 7.5R_g/L_{knot} \tag{16}$$

$$F^B_{barrier}/k_BT \approx 97.4R_g/L_{knot} - 1.13 \tag{17}$$

We use a single-parameter fit in eq 16 so that we can compare it with eq 15. This comparison suggests that a knot with the size L_{knot} is equivalent to a pore with a diameter

$$d^{equivalent}_{pore} \approx L_{knot}/7.5 \tag{18}$$

in the term of imposing a free energy barrier for a polymer. The coefficient of 7.5 appears to be a reasonable value. Our previous theoretical study[44] suggests that the polymer segments in the knot core are effectively confined inside a virtual tube with a diameter of $D_{tube} \approx L_{knot}/16$. The open area may be considered to have a dimension of $2D_{tube} \approx L_{knot}/8$, which is close to eq 18. It is worth pointing out that mapping the knot with a side chain to the pore translocation of a polymer is a crude approximation, because the shape of the knot is far from a regular circle. Moreover, the polymer segments in the knot core always undergo thermal motion, and accordingly, the pore produced by a knot core is a dynamic pore.

4. CONCLUSIONS

In summary, we perform Langevin dynamics simulations to investigate the effects of side chains on polymer knots. We find that side chains act as barriers and lead to the stepwise diffusion of a knot along a polymer. Surprisingly, we find that how a knot crosses a side chain resembles how a tethered polymer translocates through a pore. Inspired by the latter case, we find a simple linear expression for the free energy barrier caused by a side chain. On the basis of the free energy barrier, the diffusion coefficient of a knot in the presence of side chains is also derived.

Our results should provide insights to the understanding of knots in peptides, where side chains are common. Previous studies have performed simulations to investigate knotted proteins using coarse-grained models,[49,50] which applied bead–bead attractions and hence are different from the current polymer model with pure repulsions between beads. Furthermore, our empirical expressions can guide the rational control of knot diffusion on a stretched polymer by tuning the length and density of side chains. The relevant experiments can be performed on branched DNA molecules, which were recently synthesized by the Schroeder group.[51] Note that the current study focuses on the large-gap regime where the gap between two side chains is larger than the knot size. It is of great interest to investigate the small-gap regime, i.e., high grafting density, which is close to the case of peptides. In addition, the current study only considers flexible chains in the backbone and side chains and uses the same size for all beads in the backbone and side chains. It is also of great interest to explore the effects of side chains with varying bending stiffness and bead sizes, considering the different sizes of side chains among amino acids. It would be interesting to examine whether the approximate linear relationship still holds for the small gap regime and side chains with bending stiffness.

The barriers caused by side chains that slow down knot diffusion on a stretched polymer also resemble molecular friction caused by the surface roughness of molecules. Such similarity suggests that knot diffusion on a branched polymer may be used to investigate molecular friction. The surface roughness can be tuned through the length and density of the side chains. It may be convenient to tune the compression force for friction through adjusting the tension at the ends of polymer, which controls the knot size and then controls the contact between the side chain and the segments inside the knot core.

DOI: 10.1021/acs.macromol.9b01425
Macromolecules 2019, 52, 6792−6800

■ ASSOCIATED CONTENT

Supporting Information

The Supporting Information is available free of charge on the ACS Publications website at DOI: 10.1021/acs.macromol.9b01425.

More details about the radius of gyration of a polymer in the vicinity of a pore and in free space; translocation of a tethered polymer through a pore; exponential distribution of the lifetimes of a knot in the states A and B (PDF)

■ AUTHOR INFORMATION

Corresponding Author

*E-mail: pdoyle@mit.edu.

ORCID

Liang Dai: 0000-0002-4672-6283

Beatrice W. Soh: 0000-0001-8399-5995

Patrick S. Doyle: 0000-0003-2147-9172

Notes

The authors declare no competing financial interest.

■ ACKNOWLEDGMENTS

This research is financially supported by City University of Hong Kong through the start-up project (Project No. 9610420), the National Natural Science Foundation of China (Project No. 21973080), and the National Science Foundation (Grant CBET-1602406).

■ REFERENCES

(1) Rybenkov, V. V.; Cozzarelli, N. R.; Vologodskii, A. V. Probability of DNA knotting and the effective diameter of the DNA double helix. *Proc. Natl. Acad. Sci. U. S. A.* **1993**, *90*, 5307−5311.

(2) Shaw, S. Y.; Wang, J. C. Knotting of a DNA chain during ring closure. *Science* **1993**, *260*, 533−536.

(3) Taylor, W. R. A deeply knotted protein structure and how it might fold. *Nature* **2000**, *406*, 916−919.

(4) Jamroz, M.; Niemyska, W.; Rawdon, E. J.; Stasiak, A.; Millett, K. C.; Sułkowski, P.; Sulkowska, J. I. KnotProt: a database of proteins with knots and slipknots. *Nucleic Acids Res.* **2015**, *43*, D306−D314.

(5) Christian, T.; Sakaguchi, R.; Perlinska, A. P.; Lahoud, G.; Ito, T.; Taylor, E. A.; Yokoyama, S.; Sulkowska, J. I.; Hou, Y.-M. Methyl transfer by substrate signaling from a knotted protein fold. *Nat. Struct. Mol. Biol.* **2016**, *23*, 941−948.

(6) Ziegler, F.; Lim, N. C.; Mandal, S. S.; Pelz, B.; Ng, W.-P.; Schlierf, M.; Jackson, S. E.; Rief, M. Knotting and unknotting of a protein in single molecule experiments. *Proc. Natl. Acad. Sci. U. S. A.* **2016**, *113*, 7533.

(7) San Martín, Á.; Rodriguez-Aliaga, P.; Molina, J. A.; Martin, A.; Bustamante, C.; Baez, M. Knots can impair protein degradation by ATP-dependent proteases. *Proc. Natl. Acad. Sci. U. S. A.* **2017**, *114*, 9864.

(8) Marcos, V.; Stephens, A. J.; Jaramillo-Garcia, J.; Nussbaumer, A. L.; Woltering, S. L.; Valero, A.; Lemonnier, J.-F.; Vitorica-Yrezabal, I. J.; Leigh, D. A. Allosteric initiation and regulation of catalysis with a molecular knot. *Science* **2016**, *352*, 1555−1559.

(9) Zhang, L.; Stephens, A. J.; Nussbaumer, A. L.; Lemonnier, J.-F.; Jurček, P.; Vitorica-Yrezabal, I. J.; Leigh, D. A. Stereoselective synthesis of a composite knot with nine crossings. *Nat. Chem.* **2018**, *10*, 1083.

(10) Arai, Y.; Yasuda, R.; Akashi, K.-i.; Harada, Y.; Miyata, H.; Kinosita, K., Jr; Itoh, H. Tying a molecular knot with optical tweezers. *Nature* **1999**, *399*, 446.

(11) Tang, J.; Du, N.; Doyle, P. S. Compression and self-entanglement of single DNA molecules under uniform electric field. *Proc. Natl. Acad. Sci. U. S. A.* **2011**, *108*, 16153−16158.

(12) Renner, C. B.; Doyle, P. S. Stretching self-entangled DNA molecules in elongational fields. *Soft Matter* **2015**, *11*, 3105−3114.

(13) Rosa, A.; Di Ventra, M.; Micheletti, C. Topological jamming of spontaneously knotted polyelectrolyte chains driven through a nanopore. *Phys. Rev. Lett.* **2012**, *109*, 118301.

(14) Arsuaga, J.; Vazquez, M.; Trigueros, S.; Sumners, D. W.; Roca, J. Knotting probability of DNA molecules confined in restricted volumes: DNA knotting in phage capsids. *Proc. Natl. Acad. Sci. U. S. A.* **2002**, *99*, 5373−5377.

(15) Arsuaga, J.; Vazquez, M.; McGuirk, P.; Trigueros, S.; Sumners, D. W.; Roca, J. DNA knots reveal a chiral organization of DNA in phage capsids. *Proc. Natl. Acad. Sci. U. S. A.* **2005**, *102*, 9165.

(16) Matthews, R.; Louis, A.; Yeomans, J. Knot-controlled ejection of a polymer from a virus capsid. *Phys. Rev. Lett.* **2009**, *102*, No. 088101.

(17) Marenduzzo, D.; Micheletti, C.; Orlandini, E.; Sumners, D. W. Topological friction strongly affects viral DNA ejection. *Proc. Natl. Acad. Sci. U. S. A.* **2013**, *110*, 20081−20086.

(18) Micheletti, C.; Marenduzzo, D.; Orlandini, E. Polymers with spatial or topological constraints: Theoretical and computational results. *Phys. Rep.* **2011**, *504*, 1−73.

(19) Orlandini, E. Statics and dynamics of DNA knotting. *J. Phys. A: Math. Theor.* **2018**, *51*, No. 053001.

(20) Micheletti, C.; Orlandini, E. Knotting and metric scaling properties of DNA confined in nano-channels: a Monte Carlo study. *Soft Matter* **2012**, *8*, 10959.

(21) Micheletti, C.; Orlandini, E. Knotting and unknotting dynamics of DNA strands in nanochannels. *ACS Macro Lett.* **2014**, *3*, 876−880.

(22) Dai, L.; van der Maarel, J. R.; Doyle, P. S. Effect of nanoslit confinement on the knotting probability of circular DNA. *ACS Macro Lett.* **2012**, *1*, 732−736.

(23) Dai, L.; Renner, C. B.; Doyle, P. S. Metastable knots in confined semiflexible chains. *Macromolecules* **2015**, *48*, 2812−2818.

(24) Amin, S.; Khorshid, A.; Zeng, L.; Zimny, P.; Reisner, W. A nanofluidic knot factory based on compression of single DNA in nanochannels. *Nat. Commun.* **2018**, *9*, 1506.

(25) Micheletti, C.; Marenduzzo, D.; Orlandini, E.; Sumners, D. Simulations of knotting in confined circular DNA. *Biophys. J.* **2008**, *95*, 3591−3599.

(26) Marenduzzo, D.; Orlandini, E.; Stasiak, A.; Sumners, D. W.; Tubiana, L.; Micheletti, C. DNA−DNA interactions in bacteriophage capsids are responsible for the observed DNA knotting. *Proc. Natl. Acad. Sci. U. S. A.* **2009**, *106*, 22269−22274.

(27) Huang, L.; Makarov, D. E. Langevin dynamics simulations of the diffusion of molecular knots in tensioned polymer chains. *J. Phys. Chem. A* **2007**, *111*, 10338−10344.

(28) Bao, X. R.; Lee, H. J.; Quake, S. R. Behavior of complex knots in single DNA molecules. *Phys. Rev. Lett.* **2003**, *91*, 265506.

(29) Renner, C. B.; Doyle, P. S. Untying knotted DNA with elongational flows. *ACS Macro Lett.* **2014**, *3*, 963−967.

(30) Narsimhan, V.; Klotz, A. R.; Doyle, P. S. Steady-state and transient behavior of knotted chains in extensional fields. *ACS Macro Lett.* **2017**, *6*, 1285−1289.

(31) Soh, B. W.; Narsimhan, V.; Klotz, A. R.; Doyle, P. S. Knots modify the coil−stretch transition in linear DNA polymers. *Soft Matter* **2018**, *14*, 1689−1698.

(32) Soh, B. W.; Klotz, A. R.; Doyle, P. S. Untying of Complex Knots on Stretched Polymers in Elongational Fields. *Macromolecules* **2018**, *51*, 9562−9571.

(33) Klotz, A. R.; Soh, B. W.; Doyle, P. S. Motion of Knots in DNA Stretched by Elongational Fields. *Phys. Rev. Lett.* **2018**, *120*, 188003.

(34) Matthews, R.; Louis, A. A.; Likos, C. N. Effect of Bending Rigidity on the Knotting of a Polymer under Tension. *ACS Macro Lett.* **2012**, *1*, 1352−1356.

(35) Poier, P.; Likos, C. N.; Matthews, R. Influence of Rigidity and Knot Complexity on the Knotting of Confined Polymers. *Macromolecules* **2014**, *47*, 3394.

(36) Dai, L.; Doyle, P. S. Effects of intrachain interactions on the knot size of a polymer. *Macromolecules* **2016**, *49*, 7581−7587.

DOI: 10.1021/acs.macromol.9b01425
Macromolecules 2019, 52, 6792−6800

(37) Dai, L.; Doyle, P. S. Trapping a Knot into Tight Conformations by Intra-Chain Repulsions. *Polymers* **2017**, *9*, 57.
(38) Dai, L.; Doyle, P. S. Universal Knot Spectra for Confined Polymers. *Macromolecules* **2018**, *51*, 6327−6333.
(39) D'Adamo, G.; Micheletti, C. Molecular crowding increases knots abundance in linear polymers. *Macromolecules* **2015**, *48*, 6337−6346.
(40) Plesa, C.; Verschueren, D.; Pud, S.; van der Torre, J.; Ruitenberg, J. W.; Witteveen, M. J.; Jonsson, M. P.; Grosberg, A. Y.; Rabin, Y.; Dekker, C. Direct observation of DNA knots using a solid-state nanopore. *Nat. Nanotechnol.* **2016**, *11*, 1093−1097.
(41) Suma, A.; Micheletti, C. Pore translocation of knotted DNA rings. *Proc. Natl. Acad. Sci. U. S. A.* **2017**, *114*, No. E2991.
(42) Grosberg, A. Y.; Rabin, Y. Metastable tight knots in a wormlike polymer. *Phys. Rev. Lett.* **2007**, *99*, 217801.
(43) Grosberg, A. Y. Do knots self-tighten for entropic reasons? *Polym. Sci., Ser. A* **2016**, *58*, 864−872.
(44) Dai, L.; Renner, C. B.; Doyle, P. S. Metastable tight knots in semiflexible chains. *Macromolecules* **2014**, *47*, 6135−6140.
(45) Dai, L.; Renner, C. B.; Doyle, P. S. Origin of Metastable Knots in Single Flexible Chains. *Phys. Rev. Lett.* **2015**, *114*, No. 037801.
(46) Plimpton, S. Fast parallel algorithms for short-range molecular dynamics. *J. Comput. Phys.* **1995**, *117*, 1−19.
(47) Palyulin, V. V.; Ala-Nissila, T.; Metzler, R. Polymer translocation: the first two decades and the recent diversification. *Soft Matter* **2014**, *10*, 9016.
(48) Narsimhan, V.; Renner, C. B.; Doyle, P. S. Jamming of Knots along a Tensioned Chain. *ACS Macro Lett.* **2016**, *5*, 123−127.
(49) Sułkowska, J. I.; Sułkowski, P.; Szymczak, P.; Cieplak, M. Stabilizing effect of knots on proteins. *Proc. Natl. Acad. Sci. U. S. A.* **2008**, *105*, 19714.
(50) Sułkowska, J. I.; Sułkowski, P.; Szymczak, P.; Cieplak, M. Untying knots in proteins. *J. Am. Chem. Soc.* **2010**, *132*, 13954−13956.
(51) Mai, D. J.; Marciel, A. B.; Sing, C. E.; Schroeder, C. M. Topology-controlled relaxation dynamics of single branched polymers. *ACS Macro Lett.* **2015**, *4*, 446−452.

DOI: 10.1021/acs.macromol.9b01425
Macromolecules 2019, 52, 6792−6800